Mon. Not. R. Astron. Soc. **366,** L1–L5 (2006) doi:10.1111/j.1745-3933.2005.00118.x

VIMOS-VLT and *Spitzer* observations of a radio galaxy at $z = 2.5^{\star}$

M. Villar-Martín,[1]† S. F. Sánchez,[2] C. De Breuck,[3] R. Peletier,[4] J. Vernet,[3] A. Rettura,[3,5] N. Seymour,[6] A. Humphrey,[7] D. Stern,[8] S. di Serego Alighieri[9] and R. Fosbury[10]

[1]*Instituto de Astrofísica de Andalucía (CSIC), Aptdo. 3004, 18080 Granada, Spain*
[2]*Centro Astronómico Hispano Alemán de Calar Alto, E4004 Almería, Spain*
[3]*European Southern Observatory, Karl Schwarschild Str, 2, D-85748 Garching bei München, Germany*
[4]*Kapteyn Astronomical Institute, University of Groningen, Postbus 800, 9700 AV Groningen, the Netherlands*
[5]*Université Paris-Sud 11, Rue Georges Clemenceau 15, Orsay, F-91405, France*
[6]*Spitzer Science Center, California Institute of Technology, Mail Code 220-6, 1200 East California Boulevard Pasadena, CA 91125 USA*
[7]*Department of Physical Sciences, University of Hertfordshire, College Lane, Hatfield, Herts AL10 9AB*
[8]*Jet Propulsion Laboratory, California Institute of Technology, MS 169-506, Pasadena, CA 91109, USA*
[9]*INAF-Osservatorio Astrofisico di Arcetri, Largo Enrico Fermi 5, I-50125 Firenze, Italy*
[10]*ST-ECF, Karl-Schwarzschild Str. 2, 85748 Garching bei München, Germany*

Accepted 2005 October 25. Received 2005 October 25; in original form 2005 September 05

ABSTRACT

We present: (i) a kinematic and morphological study of the giant Lyα nebula associated with the radio galaxy MRC 2104−242 ($z = 2.49$) based on integral field spectroscopic Visible Multiobject Spectrograph (VIMOS) data from the Very Large Telescope (VLT), and (ii) a photometric study of the host (proto?) galaxy based on *Spitzer Space Telescope* data. The galaxy appears to be embedded in a giant ($\gtrsim$120 kpc) gas reservoir that surrounds it completely. The kinematic properties of the nebula suggest that it is a rotating structure, which would imply a lower limit to the dynamical mass of $\sim 3 \times 10^{11}\,\mathrm{M}_{\odot}$. An alternate scenario is that the gas is infalling. Such a process would be able to initiate and sustain significant central starburst activity, although it is likely to contribute with less than 10 per cent of the total stellar mass.

The near- to mid-infrared spectral energy distribution of the radio galaxy suggests the existence of a reddened, $E(B-V) = 0.4 \pm 0.1$, evolved stellar population of age $\gtrsim$1.8 Gyr and mass $(5 \pm 2) \times 10^{11}\,\mathrm{M}_{\odot}$. The implied formation redshift is $z_{\mathrm{f}} \gtrsim 6$. This stellar mass is similar to the stellar masses found for massive early-type galaxies at $z \sim 2$ in deep, near-infrared surveys.

Key words: galaxies: active – galaxies: evolution – galaxies: individual: MRC 2104−242.

1 INTRODUCTION

In a study based on long-slit, medium resolution ($R \sim 700$) Keck II/Very Large Telescope (VLT) spectroscopy of a sample of 10 ultrasteep spectrum, high-redshift ($z \sim 2.5$) radio galaxies (HzRGs), we found that these objects are embedded in giant (often $\geqslant$100 kpc), low surface brightness haloes of metal-rich, ionized gas with *quiescent kinematics* (Villar-Martín et al. 2003, hereafter VM03). By 'quiescent', we mean that the kinematics do not appear to be perturbed by interactions between the radio and optical structures. The haloes usually extend well beyond the brighter, perturbed regions and sometimes beyond the radio structures. We proposed that the quiescent haloes are the gas reservoirs from which the galaxies started to form and might still be forming. At some point, an active nucleus switches on and the halo becomes observable thanks to strong line emission powered by the ionizing continuum.

Our work was seriously limited by the lack of spatial information in directions other than the radio axis, through which the long slits were aligned. For this reason, we are carrying out a programme of 3D integral field spectroscopy to characterize the morphological, kinematic and ionization properties in two spatial dimensions of the extended ionized gas in a sample of powerful radio galaxies at $z \sim 2$–3.

In this Letter, we present the results obtained for the radio galaxy MRC 2104−242 at $z = 2.49$ (McCarthy et al. 1990). The radio source has an angular extent of 24 arcsec (∼200 kpc). The *Hubble Space Telescope* (*HST*) images (Pentericci et al. 2001) show that the host galaxy is very clumpy. A filamentary component more than 2 arcsec long is found aligned with the radio axis to within a few degrees.

The existence of an evolved stellar population in HzRGs has been subject of intensive study for the last two decades. The

⋆Based on observations carried out at the European Southern Observatory, Chile (programs 073.B-0189, 065.P-0579 and 075.B-0729). and with the Spitzer Space Telescope.
†E-mail: montse@iaa.es

ultraviolet and optical rest-frame spectroscopic studies have only marginally detected the continuum, which may still contain a significant non-stellar contribution (Vernet et al. 2001). To detect the old stellar population we need to observe at rest-frame near-infrared (near-IR) wavelengths. This is one of the scientific goals of the Cycle 1 *Spitzer* survey of 70 high-redshift radio galaxies (P.I. Stern, program ID 3329). We present results for MRC 2104−242 in this paper.

A $\Omega_\Lambda = 0.73$, $\Omega_m = 0.27$ and $H_0 = 71$ km s^{-1} Mpc^{-1} cosmology is adopted in this paper.

2 OBSERVATIONS AND DATA REDUCTION

The spectroscopic observations were made on UT 2004 June 17 [European Space Observatory (ESO) programme 073.B-0189(A)] using the Visible Multiobject Spectrograph (VIMOS; Le Févre et al. 2003), on the Nasmyth focus of the UT3 VLT unit. The instrument is equipped with an integral field unit made of 1600 microlenses coupled to fibres, covering 27 × 27 arcsec^2 on the sky with 0.67-arcsec diameter fibres for the high spectral resolution mode. The HR_{blue} grating was used, with an effective wavelength range ∼4150–6200 Å and an instrumental profile 3.0 ± 0.5 Å. The total integration time was 4.5 hr (9 × 1800 s). The seeing full width at half maximum (FWHM) during the observations was in the range ∼1.0–1.4 arcsec.

The data were reduced using a modified version of P3D (Becker 2002), in addition to our own software optimized for VIMOS data (Sánchez & Cardiel 2005). The data were bias-subtracted. The expected locations of the spectra were traced on a continuum-lamp exposure obtained before each target exposure. The fibre-to-fibre response at each wavelength was determined from a continuum-lamp exposure. Wavelength calibration was performed using arc lamp spectra and the telluric emission lines in the science data. After these basic reduction steps, a data cube was created for each exposure. The cubes were then recentred spatially by determining the centroid of a nearby star at each wavelength. This recentering corrects for differential atmospheric refraction. The cubes were then combined using IRAF tasks, masking the broken and/or low sensitivity fibres. A 3σ clipping algorithm removed cosmic rays. The sky background spectrum was estimated before subtraction by averaging spectra of object-free areas of the data cube. The flux calibration was performed using the long slit Focal Reducer Low Dispersion Spectrograph (FORS)-VLT spectrum discussed in VM03. Cross-talk effects were found to be negligible. These were evaluated using the field star in the VIMOS field-of-view. The fibre to fibre contamination was found to be <5 per cent for adjacent spectra in the CCD, dropping to less than 0.1 per cent for the third adjacent spectra.

To overlay the radio core position (Carilli et al. 1997) on the Lyα image, we used the Near Infrared Camera Multiobject Spectrometer (NICMOS) *HST* image, where the radio core was assumed to coincide with the IR peak. This is probably not the case if the nucleus is heavily reddened. The NICMOS peak position in the Lyα image was then calculated using a bright star that is present in both images. The 1σ uncertainty in the Lyα–radio registration is ∼0.3 arcsec.

Details about the observations and data reduction for the *Spitzer* data will be presented by Seymour et al. (in preparation). Briefly, for MRC 2104−242, we obtained 3.6-, 4.5-, 5.8- and 8.0-μm images on UT 2004 October 27 using the Infrared Array Camera (IRAC, Fazio et al. 2004), and a 16-μm image in 'peak-up only mode' on UT 2004 October 21 with the Infrared Spectrograph (Houck et al. 2004). The IRAC 'basic calibrated data' exposures were mosaiced using the

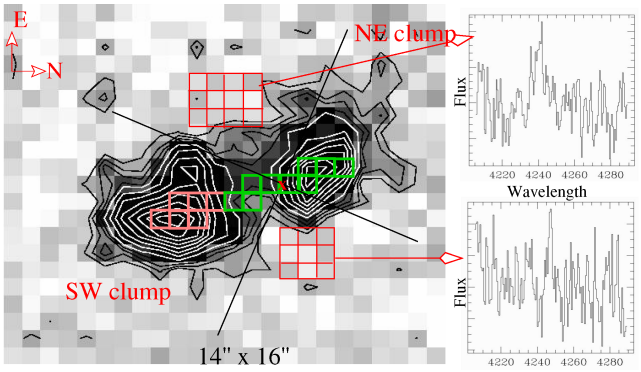

Figure 1. Lyα image of MRC 2104−242. Contours correspond to ∼5, 10, 15, 20, 25, 35, 45, 60, 70, 80, 90 and 100 per cent of the maximum contour value. Pixels marked in green and pink colours were used to extract the spectra in Fig. 2. Ionization cones with an opening angle of 90° and a vertex at the radio core position (red 'x') are shown (black lines). The spectra of two intercone regions (red squares) are also shown. Lyα is detected in both cases.

MOPEX software package (http://ssc.spitzer.caltech.edu/postbcd/) with the pixels being resampled by a factor of 2. We used SExTRACTOR (Bertin & Arnouts 1996) to measure the photometry in a matched 7-arcsec aperture defined by the 3.6-μm image. To obtain total magnitudes, we applied aperture corrections from in-flight point spread functions (Lacy et al. 2005).

3 RESULTS

A Lyα image (Fig. 1) was created by adding all the frames in the spectral direction of the data cube across the Lyα emission line spectral profile, covering the ∼4225–4260 Å spectral range. The large equivalent width of the line in all positions where it is detected ensures that the contamination by continuum emission is negligible everywhere across the image. Fig. 1 shows two spatial components (south-west, SW, and north-east, NE) separated by ∼6 arcsec, as previously described by McCarthy et al. (1990). The radio core is located between the two clumps, where Lyα presents a minimum. Similar Lyα morphologies have been observed in other HzRGs (e.g. Reuland et al. 2003). The SW component overlaps partially with the filamentary structure described in Section 1.

Low surface brightness Lyα emission is detected in regions that seem to be outside any plausible ionization cones. Two spectra were extracted from the two intercone regions shown in Fig. 1, where we have assumed a typical cone opening angle of 90° and the position of the cone vertex coinciding with the radio core. Lyα is detected in the two intercone regions. Any rotation of the axis or reasonable shift of the vertex position leads to some of the high surface brightness emission lying outside the ionization cones. McCarthy et al. (1990) mentioned the detection of a diffuse Lyα halo that surrounds the object. If the gas is ionized (but see Villar-Martín, Binette & Fosbury 1996), the ionization mechanism is an open question. Hot young stars and cooling radiation are two interesting possibilities.

3.1 Lyα kinematics

Our goal is to map the 2D kinematic field of the quiescent gas (i.e. non-perturbed by jet-induced shocks) and use it as a source of information about its origin and the formation process of the galaxy. If the gas motions are gravitational, we can constrain the dynamical mass of the system. Because of the high sensitivity of

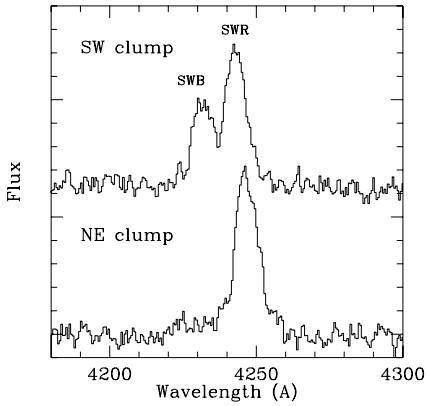

Figure 2. 1D Lyα VIMOS spectra extracted from the NW and SE clumps, using the regions shown in Fig. 1. The flux levels have been shifted for clarity. The clear split observed in the SW Lyα profile is due to kinematics. We argue that the SWR and NE components are both quiescent gas.

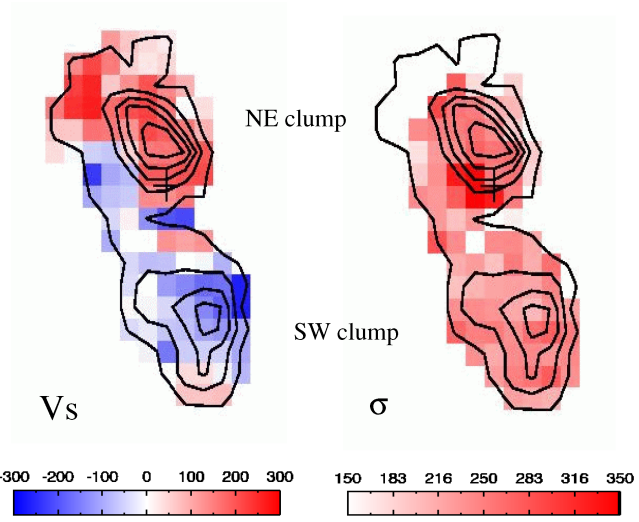

Figure 3. Overlay of the VIMOS Lyα intensity contours of the quiescent gas (i.e. components NE and SWR) with the Lyα velocity field (left) and line width σ (right). The position of the radio core is indicated with a cross. Zero velocity corresponds to a redshift $z = 2.490$. The velocity field appears symmetric and ordered, suggesting either rotation or radial flows.

Lyα to absorption by H I, it is often an unreliable kinematic tracer. Given the low signal-to-noise ratio (S/N) of the data, we cannot use other reliable tracers, such as the He sc ii λ1640 line. Instead, we have compared the integral field results here with our earlier kinematic study (VM03) based on FORS2-VLT moderate resolution (6 Å) long slit spectroscopy, which made use of both Lyα and He II.

We show in Fig. 2 the 1D VIMOS spectra of the SW and NE clumps using two apertures (see Fig. 1) matching as much as possible apertures 4 and 3 of VM03. Lyα in the SW clump is split into two components [blue (SWB) and red (SWR)], both of which are well represented by Gaussian profiles. The FWHM values are 470 $\pm$ 20 and 550 $\pm$ 20 km s^{-1}, respectively. They are separated by 820 $\pm$ 20 km s^{-1}. The line in the NE component is well represented by a Gaussian profile of FWHM 630 $\pm$ 20 km s^{-1} redshifted by 250 $\pm$ 10 km s^{-1} relative to the SWR component. These results are in good agreement with those obtained with the FORS2-VLT data. In particular, the He II line in the VM03 long-slit spectrum of the SW clump shows the same split as seen in the current VIMOS Lyα profile. Since the He II line is much less susceptible to absorption, this implies that the double structure is due to kinematics rather than absorption.

We argue that the red Lyα component from the SW clump (SWR) and the Lyα emission from the NE clump are emitted by quiescent gas. The remarkable similarity in the kinematic properties (see below) of these two components strongly suggests that the gas in both regions follows a similar kinematic pattern with the same origin. On the other hand, the sharp and large velocity shift of the SWB component suggests that this is a different, decoupled kinematic component. Although detected almost all over the SW clump, this component is strongest relative to the SWR component in pixels adjacent and coincident with the filamentary structure (Section 1), where strong evidence for jet-gas interactions exist (Humphrey et al. 2005), suggesting that it is emitted by perturbed gas.

We find that the Lyα profile of the quiescent gas is not strongly distorted by absorption. VM03 found that in general, although the kinematic measurements (FWHM and velocity shifts) for Lyα and He II can be rather different for the perturbed gas (usually broad lines), they are are in good agreement within the errors for the quiescent gas. This is also the case for MRC 2104−242 (see fig. 7, VM03). Therefore, the quiescent Lyα emission is less affected by absorption, probably due to the narrowness of the lines.

In summary, the Lyα emission from the quiescent gas (components NE and SWR) can be isolated in MRC 2104−242 at each spatial location and it can be used as a reliable kinematic tracer.

We now analyse the velocity field of the quiescent gas. The Lyα profile was fitted at each spatial pixel with Gaussian profiles. The results are shown in Fig. 3 (left) with the intensity contours of the quiescent gas overplotted. The errors are $<$30 km s^{-1} for most pixels. The velocity dispersion σ map (corrected for instrumental broadening) is also shown (Fig. 3, right). The error is estimated to be $<$60 km s^{-1}.

The kinematic pattern is rather symmetric and apparently ordered. The overall velocity field is very suggestive of a rotating structure, for which the half-amplitude of the rotation curve is $v_{\rm rot} \sim 150$ km s^{-1}. The σ map is quite featureless, with $\sigma \sim 200$–280 km s^{-1} for most spatial positions, with little noticeable difference between the two clumps other than a slight broadening of the line near the radio core. If the active nucleus coincides with the dynamical centre of the system, this line broadening further supports rotation.

3.2 Spitzer data

Table 1 presents the *Spitzer* photometry for MRC 2104−242, as well as near-IR photometry from ground-based (J_s, K_s) Infrared Spectrometer and Array Camera (ISAAC)-VLT [ESO programme 075.B-0729(B)] and *HST* (F160W) images. We have corrected the near-IR photometry for emission line contamination using archival VLT/ISAAC *JHK* spectroscopy [ESO programme 65.P-0579(A)]. We determine the contributions to the total flux to be 15 $\pm$ 5, 76 $\pm$ 5 and 51 $\pm$ 5 per cent in J_s, H and K_s, respectively.

Fig. 4 plots the near- to mid-IR spectral energy distribution (SED). The SED shows a clear rise between the K- and IRAC 3.6-μm bands, and again between 8.0 and 16 μm. We now argue that the 3.6- to 5.8-μm points are dominated by an old stellar population. Fig. 4 shows that the upturn in the SED between 8.0 and 16 μm (see Table 1) is unlikely to be explained by a stellar population; the 16-μm point is most likely dominated by warm dust emission associated with the active nucleus. We assume the 16-μm point can be fitted with a simple power law of slope −3 (Fig. 4), as determined

Table 1. Near- to mid-IR photometry of MRC 2104−242. The J_sHK_s photometry has been corrected for line emission (see text).

Band	λ_{cent} (μm)	FWHM (μm)	f_ν (μJy)
J_s	1.2	0.16	4.1 ± 1.5
F160W	1.6	0.43	1.7 ± 1.2
K_s	2.2	0.27	4.8 ± 1.8
3.6 μm	3.6	0.7	27 ± 3
4.5 μm	4.5	0.99	29 ± 3
5.8 μm	5.7	0.90	32 ± 7
8.0 μm	8.0	2.8	$\leqslant 35$
16.0 μm	16.0	6.0	72 ± 18

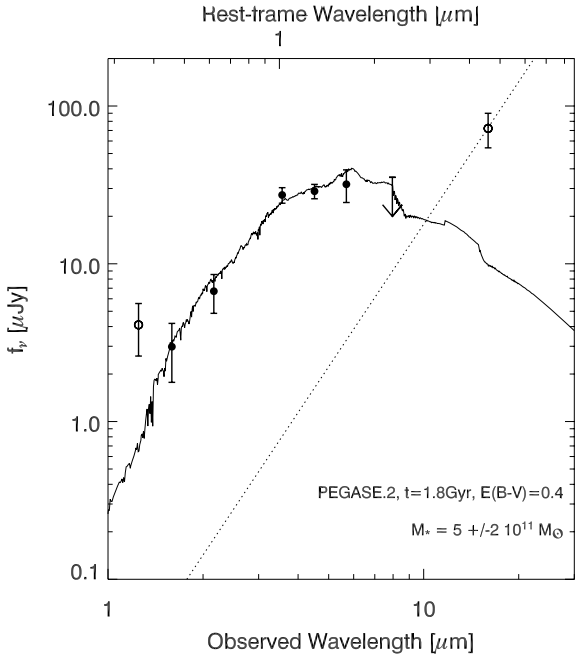

Figure 4. Near- to mid-IR SED of MRC 2104−242. The best fit is produced by a reddened, relatively evolved population of age 1.8–2.5 Gyr and stellar mass $(5 \pm 2) \times 10^{11}\,M_\odot$. The J_s band point is dominated by a combination of scattered quasar, nebular continuum and young stellar emission. All of these contributions have a blue slope, and will therefore contribute $\ll$5 per cent to the IRAC photometry. A power law of index −3 (dotted line) represents the expected thermal dust emission. The figure shows that its contribution can be safely ignored below 8 μm.

from a sample of 12 radio galaxies with *Spitzer* 16- and 24-μm data (Seymour et al., in preparation). Scaling this power-law to the 16-μm point implies that we can safely ignore any thermal dust emission at $\lambda_{obs} \leqslant 8.0$ μm. This is further supported by the 8.0-μm upper limit.

Similarly, the *JHK* points allow us to constrain the combined contributions due to scattered quasar light, nebular continuum and young stellar populations. These contributions all have a blue slope, while we detect a clear rise in the SED between 2.2 and 3.6 μm. We can therefore constrain these combined contributions to $\ll$5 per cent in the IRAC bands. Note that the excess of the *J*-band flux over the model predictions (Fig. 4) and over the *H*-band measurement can only be explained by such contributions, as any old stellar population would be fainter in *J* than in *H* (especially when we invoke reddening). Hence our strongest constraint comes from the *H*-band detection. Based on rest-frame near-IR spectroscopy of low-redshift active galaxies (e.g. Sosa-Brito et al. 2001), we expect the emission line contributions to the IRAC bands to be <5 per cent.

We now use the *H* through to the 8.0-μm SED of MRC 2104−242 to derive the most probable stellar mass of the host galaxy (see e.g. Yan et al. 2005 for a detailed discussion on uncertainties). The *J*-band point is omitted as it appears to be contaminated by light associated with either the buried active galactic nucleus (AGN) or a young stellar population, and the 16-μm point is ignored as it is probably non-stellar in origin. We systematically compare the observed SED with a set of templates computed with PÉGASE.2 models (Fioc & Rocca-Volmerange 1997) via a χ^2 minimization technique. Star formation histories (SFHs), ages, masses and dust extinction are free parameters. We model simple stellar populations of different metallicities using a Salpeter (1955) initial mass function (IMF) with a lower mass limit of $0.1\,M_\odot$ and an upper mass limit of $120\,M_\odot$. We adopt SFHs that have been shown to consistently reproduce observations of $z \sim 0$ passively-evolving, early-type galaxies (Fioc & Rocca-Volmerange 1999). A more detailed description of the fitting method will be presented in Rettura et al. (in preparation).

Results of the best-fitting model are shown in Fig. 4. We estimate the errors for the mass by sampling the full probability distribution in the multidimensional parameter space. We find a best-fitting stellar mass estimate of $(5 \pm 2) \times 10^{11}\,M_\odot$ and a colour excess $E(B-V) = 0.4 \pm 0.1$. This is similar to the stellar masses found for the most massive, early-type galaxies at $z\sim2$ in deep, IR surveys (e.g. Daddi et al. 2004; Labbé et al. 2005). The best-fitting age is 2.5 Gyr, which is very close to the age of the Universe at the source redshift, (2.7 Gyr). The minimum age that still provides a reasonable (3σ) fit is 1.8 Gyr, implying a formation redshift $z_f \gtrsim 6$. Finally, we note that the SED cannot be fitted by any simple or composite stellar population without invoking substantial reddening.

4 DISCUSSION AND CONCLUSIONS

Let us assume that the giant Lyα nebula in MRC 2104−242 is supported by rotation. If its morphology maps the true gas distribution and the gas is settled on a disc, we derive an inclination angle $i \sim 75^\circ \pm 5^\circ$ relative to the plane of the sky and a dynamical mass $\sim(3.2 \pm 0.7) \times 10^{11}\,M_\odot$ within a radius of 7 arcsec (∼60 kpc). This is similar to the stellar mass inferred from the *Spitzer* data (see Section 3.2), suggesting a surprisingly small dark matter fraction. However, the derived dynamical mass is likely to be a lower limit, since the gas is expected to be anisotropically illuminated by the hidden quasar. Therefore, the disc inclination and the direction of the major axis cannot be determined.

If the giant halo in MRC 2104−242 is settled on to a well-defined disc, then $\sigma/v_{rot} < 1$, such that v_{rot} must be $\gtrsim$240 km s^{-1} and $M_{dyn} \gtrsim 8 \times 10^{11}\,M_\odot$. On the other hand, it takes several rotation periods for gas to settle into a disc. If this is the case for the giant nebula in MRC 2104−242 and we assume a minimum of three rotation periods ($P_{rot} = 2\,\pi r/v_{rot}$) for a well-ordered disc, the 2.7-Gyr age of the Universe at $z = 2.49$ requires $v_{rot} > 400$ km s^{-1} for which $M_{dyn} > 2 \times 10^{12}\,M_\odot$. A smaller value of v_{rot} would imply that the gas has not yet settled into a stable structure.

It is possible that the SW and NE clumps are two different objects rotating around a common centre (e.g. De Breuer et al. 2005). However, the fact that Lyα emission surrounds the object completely suggests that it is a single, rotating structure. If the gas is rotating, this means that giant ($r > 60$ kpc) gaseous, rotating structures (discs?) can exist already at $z \sim 2.5$. These could be the

progenitors of the giant (> several tens of kpc) rotating discs discovered around several low-redshift radio galaxies and early-type galaxies (e.g. Morganti et al. 2002). High-redshift cooling flow models for galaxy formation (e.g. Haiman, Spaans & Quataert 2000) predict the formation of a giant, rotationally supported disc as part of the process in less than 1 Gyr.

Alternatively, the general pattern of the velocity field is also suggestive of radial motions. The radio properties can discriminate between inflow and outflow. The NE radio lobe is brighter and more polarized (Pentericci et al. 2000). According to the Laing–Garrington effect (Laing 1988), this lobe is closer to the observer. Because the gas located at this side of the nucleus is the most redshifted, it must be infalling. The collapse of such a giant structure suggests that we are witnessing an early stage in the formation process of the central galaxy (e.g. Haiman et al. 2000).

Let us assume an infall velocity of $\sim$150 $\sin\alpha$ km s^{-1} and a radius $\sim$60 $\cos\alpha$ kpc, where α is the angle between the ionized cone axis and the line of sight. As this is a narrow-line radio galaxy, α is expected to be large, $\alpha \gtrsim 60^\circ$. Therefore, after $\lesssim$2.5 $\times$ 10^8 yr, the 60-kpc halo should collapse and disappear in a very small redshift interval (by $z \sim 2.2$). The existence of giant, quiescent haloes in radio galaxies at very different redshifts (Reuland 2003; Villar-Martín et al. 2005) suggests that they are long-lived structures, unless there are multiple episodes of Lyα haloes. The implication is that much larger reservoirs of invisible gas must exist and/or some mechanism must deccelerate the infall process at some point (Iono, Yun & Mihos 2004).

As in VM03, and using the geometrical information provided by the VIMOS Lyα image, we estimate an ionized gas density $n \sim 55$ cm^{-3} (see VM03 for uncertainties in this calculation) and a gaseous mass (neutral and ionized) within 60 kpc of $\sim 10^{10}\,M_\odot$. A mass deposition rate in the range $\sim$(40–250) $M_\odot$ yr^{-1} is inferred. This infall rate might be able to initiate and sustain central starburst activity at several tens of $M_\odot$ yr^{-1} (Iono et al. 2004). Because the object contains a $\geqslant$1.8-Gyr-old population as well as the young population triggered by the current inflow, at least two episodes of star formation are inferred for the formation of this massive galaxy. If the halo has $\sim 10^{10}\,M_\odot$, this is probably the maximum it will contribute to the build up of the stellar mass of the galaxy, so that the infalling gas will only be <10 per cent of the galaxy mass.

In summary, MRC 2104−242 contains an evolved stellar population that formed at $z \gtrsim 6$. The kinematic properties of the extended gas suggest that it is associated with a giant rotating structure, the remnant of the formation process of the galaxy. Alternatively, the gas might be infalling during an early phase in the galaxy formation process. Extending a similar study to a larger sample of objects will be very useful in understanding the demographics and nature of ordered kinematics in the quiescent gas associated with HzRGs.

ACKNOWLEDGMENTS

We gratefully acknowledge the SHzRG team who have provided the *Spitzer* data presented here. The work of MVM was supported by the Spanish Ministerio de Educación y Ciencia and the Junta de Andalucía through the grants AYA2004-02703 and TIC-114. The work of DS was carried out at Jet Propulsion Laboratory, California Institute of Technology, under a contract with NASA.

REFERENCES

Becker T., 2002, PhD thesis, Univ. Potsdam
Bertin E., Arnouts S., 1996, A&ASS, 117, 393
Carilli C., Röttgering H., van Ojik R., Miley G., van Breugel W., 1997, ApJS, 109, 1
Daddi E. et al., 2004, ApJ, 600, L127
De Breuck C., Downes D., Neri R., van Breugel W., Reuland M., Omont A., Ivison R., 2005, A&A, 430, L1
Fazio G. et al., 2004, ApJS, 154, 10
Fioc M., Rocca-Volmerange B., 1997, A&A, 351, 869
Fioc M., Rocca-Volmerange B., 1999, A&A, 326, 950
Haiman Z., Spaans M., Quataert E., 2000, ApJ, 537, L5
Houck J. et al., 2004, ApJS, 154, 18
Humphrey A., Villar-Martín M., Fosbury R., Vernet J., Di Serego Alighieri S. 2005, MNRAS, submitted
Iono D., Yun M., Mihos J., 2004, ApJ, 616, 199
Lacy M. et al., 2005, ApJS, 161 41
Labbé I. et al., 2005, ApJ, 624, L81
Laing R. A., 1988, Nat, 331, 149
Le Févre O. et al., in Iye M., Moorwood A. F., eds, Proc. SPIE Vol. 4841, Instrument Design and Performance for Optical/Infrared Ground-based Telescopes. SPIE, Bellingham WA, p. 1670
McCarthy P., Kapahi V., van Breugel W., Subrahmanya C., 1990, AJ, 100, 1014
Morganti R., Oosterloo S., Tinti S., Tadhunter C. N., Wills K. A., van Moorsel G., 2002, A&A, 387, 830
Pentericci L., Van Reeven N., Carilli C., Röttgering H., Miley G. 2000, A&AS, 145, 121
Pentericci L., McCarthy P., Röttgering H., Miley G. K., van Breugel W. J. M., Fosbury R., 2001, ApJS, 135, 63
Reuland M. et al., 2003, ApJ, 592, 755
Salpeter E., 1955, ApJ, 121, 161
Sánchez S. F., Cardiel N., 2005, Calar Alto Newsletter, n.10
Sosa-Brito R., Tacconi-Garman L., Lehnert M., Gallimore J., 2001, ApJS, 136, 61
Vernet J., Fosbury R., Villar-Martín M., Cohen M. H., Cimatti A., di Serego Alighieri S., Goodrich R. W., 2001, A&A, 366, 7
Villar-Martín M., Binette L., Fosbury R., 1996, A&A, 312, 751
Villar-Martín M., Vernet J., di Serego Alighieri S., Fosbury R., Humphrey A., Pentericci L., 2003, MNRAS, 346, 273 [VM03]
Villar-Martín M., Tadhunter C., Morganti R., Holt J., 2005, MNRAS, 359, L5
Yan H. et al., 2005, ApJ, 634, 109

This paper has been typeset from a TEX/LATEX file prepared by the author.